Talanta 298 (2026) 129048

Contents lists available at ScienceDirect

Talanta

journal homepage: www.elsevier.com/locate/talanta

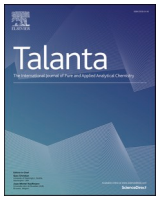

Light-triggered electrochemical biosensor using singlet oxygen for self-powered operation and glucose detection

Akhilesh Kumar Gupta, Robert Buller, Alexey V. Krasnoslobodtsev *

Department of Physics, University of Nebraska Omaha, Omaha, NE, 68182, USA

ARTICLE INFO

Keywords:
Biosensor
Light-triggered sensing
Singlet oxygen
Self-powered

ABSTRACT

This study introduces a light-activated sensing strategy that integrates photosensitization with electrochemical detection. The sensor employs Eosin Y, a photosensitizer that generates singlet oxygen ($^1O_2$) via type II photosensitization. Immobilized within a thin polymer matrix on a carbon working electrode, Eosin Y produces $^1O_2$, under green light (520 nm) illumination, initiating a redox process that yields a measurable current. To incorporate biosensing capabilities and enable self-powered operation, this $^1O_2$ – mediated process was coupled with glucose oxidase (GOx) to construct a fully operational glucose biosensor. The addition of glucose reverses the current flow by causing GOx to compete for electrons, with the resulting current magnitude correlating with glucose concentration providing a sensitive measure of glucose. The biosensor, as proof-of-principle, demonstrated excellent performance over a range of glucose concentrations (0–73 mM), achieving a detection limit (LOD) of 2.8 mM for steady state photocurrent under oxygen-saturated conditions. This platform leverages light and $^1O_2$ as stimuli for tunable, on-demand signal control, offering a novel approach for adaptive, real-time biosensing technologies.

1. Introduction

Many fields today rely on robust sensing technologies, with new applications continuously emerging. Particularly valuable are technologies that meet the evolving demands of these fields, such as on-demand, controlled activation, enabling precise measurements only when needed. This approach supports energy efficiency and minimizes power requirements. Technologies that combine such controlled sensing capability with compatibility for wearable and implantable formats are especially well positioned to meet the needs of real-world applications where low energy consumption or, ideally, self-powered operation is essential [1]. Among various biosensing modalities being developed to address these needs, electrochemical methods stand out for their low cost and simplicity compared to other detection methods [2]. In recent years, electrochemical biosensors have attracted significant attention due to their high sensitivity, specificity, and potential for miniaturization [3]. One innovative class of biosensors that offers unique advantages is photoelectrochemical biosensors, which harness light-activated processes to drive electrochemical detection [4]. These systems employ photosensitizers to precisely control signal generation through light, enabling high sensitivity and temporal resolution. Photoelectrochemical biosensing operates on the principle of photo-induced electron transfer, a newly emerging technology that has drawn growing interest [5–7]. By using light as the excitation source for detection, photoelectrochemical measurements benefit from reduced undesired background signals, increased sensitivity, cost-effectiveness, and the ease of miniaturization of detection devices [6]. In photoelectrochemical sensing, the interaction between analytes and illuminated photoelectrochemically active materials leads to changes in photocurrent [8]. The underlying mechanism involves photo-induced electron transfer, where photon absorption by a photoactive material initiates current flow [9]. A particularly promising approach involves using singlet oxygen ($^1O_2$) as the source of charges that generate current. As a highly reactive oxygen species, singlet oxygen ($^1O_2$) plays a significant role in many fields, including water disinfection [10], pollutant degradation [11], fine chemical synthesis and polymer science [12], photodynamic therapy [13], and electrochemical (bio)sensing [14]. Despite its potential, the use of $^1O_2$ for electrochemical detection of biomolecules remains largely unexplored, with only a few studies reporting this promising approach [15–17].

The controlled generation of singlet oxygen, triggered exclusively by the excitation of photosensitizers, holds significant potential. While $^1O_2$

* Corresponding author.
E-mail address: akrasnos@unomaha.edu (A.V. Krasnoslobodtsev).

https://doi.org/10.1016/j.talanta.2025.129048
Received 22 May 2025; Received in revised form 20 October 2025; Accepted 28 October 2025
Available online 30 October 2025

is not commonly considered a direct source for the current generation, it can be coupled with redox pairs, enzymes, or other elements to produce current in response to a detection event [16,18]. In this study, we introduce a novel light-triggered electrochemical biosensor for glucose detection and a potential for self-powered operation, utilizing the photophysical properties of Eosin Y as a photosensitizer. Upon light activation, Eosin Y generates singlet oxygen ($^1O_2$) through a type II photosensitization process. Singlet oxygen, a highly reactive oxygen species, subsequently interacts with glucose oxidase (GOx) in the presence of glucose, catalyzing its conversion to glucono-δ-lactone, triggering a redox cycle that generates a quantifiable signal directly correlated with glucose concentration. This approach combines the high reactivity of $^1O_2$ and the enzymatic specificity of GOx to achieve a quantifiable sensitivity to glucose. The biosensor is constructed by embedding Eosin Y within a thin polymer layer on a carbon electrode, with GOx immobilized on the surface of the polymer layer to form a coupled system. Upon laser irradiation, singlet oxygen is produced in a controlled manner, enhancing the efficiency and precision of the sensing reaction. The light-triggered activation offers fine control over the measurement process, making the system well-suited for real-time monitoring applications where low energy consumption is critical.

This paper details the biosensor's design in the single-enzyme, single-electrode configuration describing also fabrication and characterization of the device. We further explore the underlying mechanisms of $^1O_2$ generation and its role in self-powered operation and glucose detection. The biosensor's performance is evaluated in terms of sensitivity and potential applications in clinical diagnostics. By leveraging the unique properties of photoelectrochemical sensing, the light-triggered electrochemical sensor developed in this study represents a promising approach for self-powered, precise analyte detection. The results demonstrate proof-of-principle of the light activated sensing mechanism and highlight its potential to enhance the performance of biosensing technologies, particularly in clinical and wearable applications.

2. Experimental section

2.1. Materials

Glucose Oxidase (GOx) derived from Aspergillus Niger, N-(3-dimethyl aminopropyl)-N′-ethyl carbodiimide hydrochloride (EDC), Pyrrole-2-carboxylic acid (PCA), Eosin-Y (EY), D-(+) – glucose, 9,10-anthracenediyl-bis (methylene) dimalonic acid (ABDA), and ethanol were purchased from Sigma Aldrich. N-hydroxysuccinimide (NHS) was obtained from Merck. Eosin-Y (EY) is a dye produced from fluorescein by bromination and purchased from Lab Chem (USA). All chemicals were of analytical grade. All aqueous solutions were prepared in ultrahigh-quality (UHQ) water. In addition, a glucose solution was prepared at least 24 h before use to allow the glucose to undergo mutarotation and to reach equilibrium between α and β forms. A 10 mg/mL GOx solution was prepared in a phosphate saline buffer solution, and PCA was prepared in ethanol.

2.2. Device design and preparation

Screen-printed electrodes (SPE, DRP-110-U75 from Metrohm USA, Inc.) with a working carbon electrode surface area of 0.12566 cm^2 were used in this study. To deposit the EY-PCA composite on the SPEs, a 50-cycle cyclic voltammetry (CV) process was performed, Fig. S1. Under optimized conditions, the SPE was placed in an electrochemical cell containing 3.25 mL of a solution comprising 5 mM EY and 35 mM PCA. The potential was scanned at a rate of 100 mV/s over a range of −2.0 V to +1.8 V for 50 cycles controlled with a potentiostat (Ossila, T2006B1-US), resulting in the formation of an EY-PCA composite on the surface of the SPE working electrode. Following the synthesis, the composite electrode (EY–PCA) was rinsed with water and dried. To functionalize the electrode with glucose oxidase (GOx), the modified SPE was first treated with a mixture of 0.2 M EDC and 0.1 M NHS solutions and incubated for 30 min at ambient temperature. The electrode was then rinsed with deionized water and immediately treated with a 10 mg/mL GOx solution, which resulted in covalent attachment of the GOx enzyme to the top surface layer of the modified electrode (EY–PCA) via amide bond formation, forming the working electrode completely functionalized with nanocomposite (EY–PCA/GOx).

2.3. Chronoamperometric measurements

The SPE electrodes, modified with the EY-PCA/GOx nanocomposite, were employed for chronoamperometric measurements. A three-electrode setup was used for chronoamperometric measurements. A PBS buffer solution (pH 7.4) served as the electrolyte. For chronoamperometry, after the system reached stability, a glucose solution was added incrementally by volume to the electrochemical cell. During chronoamperometric measurements, the potential was maintained at 0.5 V and the current versus time response was recorded using the same potentiostat. Green laser light (520 nm, Laser Diode L520P50, from Thorlabs, Inc.) was used to illuminate the system, with its power calibrated via an optical power meter (PM100D from Thorlabs, Inc.). Measurements were conducted under controlled light-chopping conditions, alternating 20 s of laser OFF and 20 s ON to ensure uniformity. The ON/OFF switching was triggered manually for precise control. Stability and reproducibility tests were conducted, with the corresponding results shown in Fig. S4B and S4C, respectively.

2.4. Electron paramagnetic resonance spectroscopy

Electron Paramagnetic Resonance (EPR) spectroscopy was used to investigate the generation of reactive species by Eosin Y (EY) in the presence of a spin trap. The spin trap, 1-hydroxy-3-carboxy-2,2,5,5-tetramethylpyrrolidine (CPH), served as a sensitive probe for detecting reactive oxygen species (ROS) and free radicals. Two conditions were explored: 1) *without laser irradiation (as control):* a sample containing Eosin Y (10 μM) and CPH (200 μM) was kept in the dark and measurements were performed while minimizing the exposure of the sample to light; 2) *with laser irradiation*: a similar sample was exposed to continuous green laser light (520 nm) for the duration of 2 min before the EPR measurements were performed. The laser power was adjusted to 14 mW/cm^2 as assessed by the optical power meter (PM100D from Thorlabs, Inc.). EPR spectra were recorded using a Bruker E-Scan EPR spectrometer. The emergence of a non-zero EPR signal after light irradiation was attributed to the ability of Eosin Y to generate singlet oxygen.

2.5. Singlet oxygen optical detection

To evaluate the singlet oxygen ($^1O_2$) generation capability by Eosin Y (EY) as a PSII system, 9,10-anthracenediyl-bis(methylene)dimalonic acid (ABDA) was employed as a chemical probe. ABDA reacts selectively with $^1O_2$ to form an endoperoxide, resulting in a gradual decrease in its characteristic absorbance. First, a stock solution of ABDA in DMSO (~10 mM) was used to prepare ABDA solutions for measurements. Since ABDA was difficult to fully dissolve in pure water, solutions were prepared in H_2O containing 1 % (v/v) DMSO. Second, for irradiation experiments, the solutions were placed in a 10 mm path-length sub-micro cuvette (16.40F-Q-10). Irradiation at 520 nm was performed using a continuous-wave green diode laser (Laser Diode L520P50, Thorlabs, Inc.) for a designated period. Third, at regular intervals, irradiation was paused, and the absorbance spectrum was recorded using a Duetta two-in-one fluorescence and absorbance spectrometer (Horiba, Inc.).

2.6. DFT calculations

Density Functional Theory (DFT) and its time-dependent variant (TDDFT) were carried out using the ORCA 6.0.0 suite to investigate the electronic structure and excitation properties of the system. For these studies, the hybrid exchange–correlation functional BP86 was used in combination with the def2-TZVP, a polarized split-valence basis set consistently applied to all atoms to maintain uniformity across geometry optimizations, energy computations, and spectral analyses (unless specified otherwise). Solvent effects were incorporated using the conductor-like polarizable continuum model (CPCM), with water as the dielectric medium ($\varepsilon = 80.4$), to better replicate experimental conditions. Spin–orbit coupling (SOC) interactions, which are critical for intersystem crossing (ISC) analysis, were evaluated by calculating the matrix elements $\langle S_1|H_{SO}|T_j\rangle$ within ORCA. The chosen computational protocol was benchmarked against other combinations of exchange functionals and basis sets, yielding the closest agreement with experimental absorption (excitation) peak values.

3. Results and discussion

3.1. Design of the sensor

Fig. 1 illustrates the conceptual design of the biosensor platform developed in this study, which builds on our previously reported single-electrode approach for dual-mode detection system [19]. This strategy involves modifying the carbon cathode to serve as a multifunctional working electrode capable of both analyte detection and photon-triggered activation. The design leverages prior advancements in single-electrode dual-mode systems [19] and incorporates strategies from single-enzyme biofuel cells powered by glucose [20]. The developed platform uses a novel biocathode concept, resulting in a single-enzyme biosensor optimized for chronoamperometric measurements with potential for self-powered operation.

As illustrated in Fig. 1, the system features a simplified miniature screen-printed electrode (SPE) configuration, consisting of a modified working electrode (MCWE), a carbon counter electrode (CCE), and a silver reference electrode (SRE). The working electrode (WE) is modified with Eosin Y (EY) embedded in a poly(pyrrole-2-carboxylic acid) (PCA) polymer layer, deposited via 50 cycles of electrochemical co-deposition (Fig. S1). This polymer (PCA-EY) layer serves a dual role: it stabilizes the EY centers while distributing them evenly across the electrode surface, and it also enables efficient redox reactions by maintaining EY's proximity to the electrode surface. Glucose oxidase (GOx) is subsequently immobilized on top of this polymer layer using EDC-NHS coupling chemistry, ensuring stable attachment and facilitating efficient processing of glucose present in the solution [19]. Together these components form a light-activated biosensing platform that achieves efficient photon-electron coupling and enables glucose detection. The sensor architecture employs a simplified three-electrode configuration, optimized for photochemical activation and redox activity. Incorporating the light-sensitive PCA-EY hybrid matrix allows for potential activation by ambient or natural light, reducing dependence on batteries and enhancing the sensor's potential for long-term wearable use. In this study, the PCA-EY matrix enabled proof-of-principle operation of the device. Future enhancements to PCA-EY, or the development of alternative photoactive polymer matrices, could further improve electron transport and charge transfer dynamics, boosting overall performance.

3.2. Photocurrent generation

The biosensor platform demonstrates a remarkable ability to generate a photocurrent even in the absence of glucose in the solution. Without glucose, the primary substrate for glucose oxidase (GOx), no enzymatic redox reactions involving GOx are expected since the enzyme should remain inactive. However, upon illumination with light at a wavelength matching the excitation profile of Eosin Y, a distinct photocurrent is still observed. This photocurrent can be attributed to the photoactivation of Eosin Y, which, upon excitation, undergoes a type II photosensitization process to produce singlet oxygen. The formation and subsequent reduction of $^1O_2$ at the electrode surface initiate electron flow, producing a measurable current, Fig. 2C. As highly reactive oxygen species, singlet oxygen can interact with the electrode either by accepting electrons directly and transforming into less reactive species, such as superoxide (O_2^-) or, under certain conditions, directly to water [15]. This behavior underscores the role of $^1O_2$ as an active intermediate in the system, even in the absence of glucose, emphasizing the sensor's unique capability for light-driven electron transfer. Under ambient conditions, as Fig. 2A demonstrates, the peak photocurrent consistently measures around 60 nA (±3 nA) and demonstrates stability through multiple light on/off cycles. To confirm the role of oxygen in photocurrent generation, dissolved oxygen was removed by flushing the solution with argon. This caused a significant reduction in photocurrent to $I = 30 \pm 4$ nA, Fig. 2B, far below the levels observed when ambient atmospheric oxygen was present. These results provide strong evidence that singlet oxygen plays a central role in photocurrent generation, with dissolved oxygen being essential for sustaining a stable and high-intensity signal.

3.3. Glucose sensing

The glucose-sensing capability of the platform is evident from its

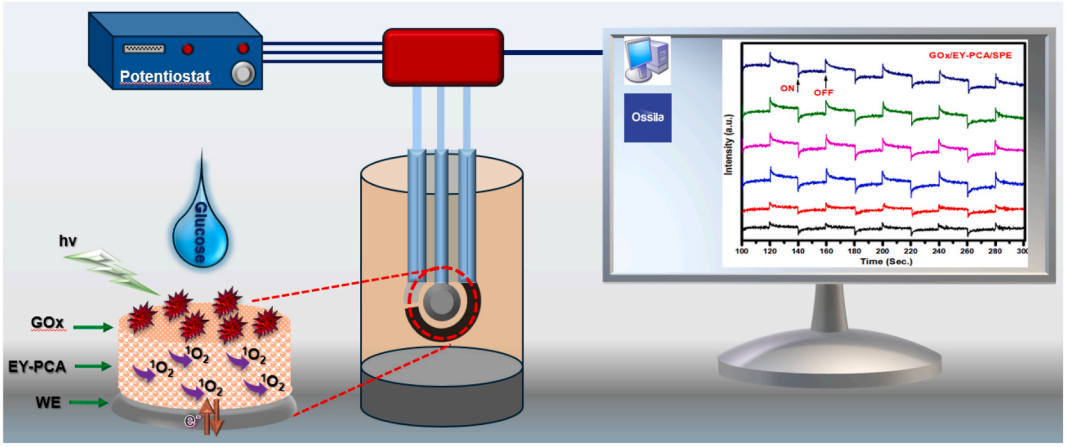

Fig. 1. Schematic illustration of the photochemical measurement setup and sensor design in a single-enzyme, single-electrode configuration, emphasizing the role of working electrode surface modification in enabling light-responsive and glucose-selective detection.

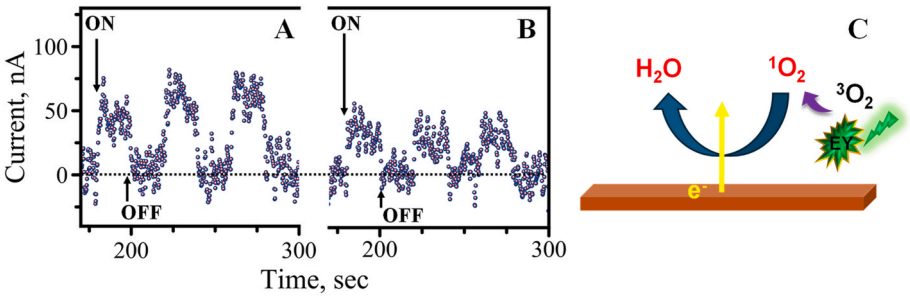

Fig. 2. Chronoamperometric traces for the last three events during the 300 s run: (A) under the ambient atmosphere conditions, (B) under argon-flushed conditions. (C) Schematic representation of the redox cycles driving electron flow and resulting in the observed positive current.

distinct and light-dependent photocurrent behavior, which shows a characteristic response upon glucose addition. The photocurrent is generated exclusively under illumination, and notably, the observed photocurrent becomes negative in the presence of glucose compared to glucose-free conditions. This current inversion is clearly illustrated in Fig. 3. Under oxygenated conditions and in the absence of glucose, the photocurrent remains stable and positive, with a magnitude of approximately I = +200 nA, as shown in Fig. S2. However, when a small amount of glucose (~1.5 mM) is introduced, the observed photocurrent switches to a negative value of I = −300 nA, Fig. 3A, resulting in a net current change of ΔI = 500 nA. This photocurrent reversal is attributed to the enzymatic activity of GOx, which catalyzes glucose oxidation, generating electrons that alter the overall current flow. As glucose concentration increases, the magnitude of the negative photocurrent also progressively intensifies, indicating a direct correlation between glucose levels and sensor signal magnitude. These results confirm that the sensor response depends on the balance between two competing processes: the positive current from light-driven singlet oxygen reduction and the negative current from GOx-mediated glucose oxidation, thereby validating the system's utility for light-activated glucose detection.

To further investigate the relationship between glucose concentration and sensor response quantitatively, glucose levels were sequentially increased from 1.5 mM to 9.2 mM, 24 mM, 45.5 mM, and finally 72.3 mM, Fig. 3A. As detailed in Fig. S2, the overall observed photocurrent arises from two competing processes: a positive signal in the absence of glucose and a negative signal in its presence. With higher glucose concentrations, the negative photocurrent becomes progressively stronger, demonstrating a clear proportional relationship between glucose concentration and photocurrent magnitude. For quantitative analysis, peak photocurrent intensities (I) were measured at each "Light ON" point and plotted against the corresponding glucose concentrations, resulting in a dataset with a strong linear correlation ($R^2 = 0.967$), as shown in Fig. 3B. Based on these data, the limit of detection (LOD) under the given experimental conditions was determined to be 11 mM, demonstrating the sensor's ability to reliably detect glucose at concentrations near or above this threshold. Remarkably, the sensor achieves this functionality without relying on external power sources. Instead, it utilizes light energy and glucose as dual inputs, potentially enabling the development of a self-powered detection mechanism. This unique attribute makes the sensor particularly well-suited for energy-efficient and portable biosensing applications.

Closer analysis revealed two distinct components in the generated photocurrent signal which became increasingly apparent at higher

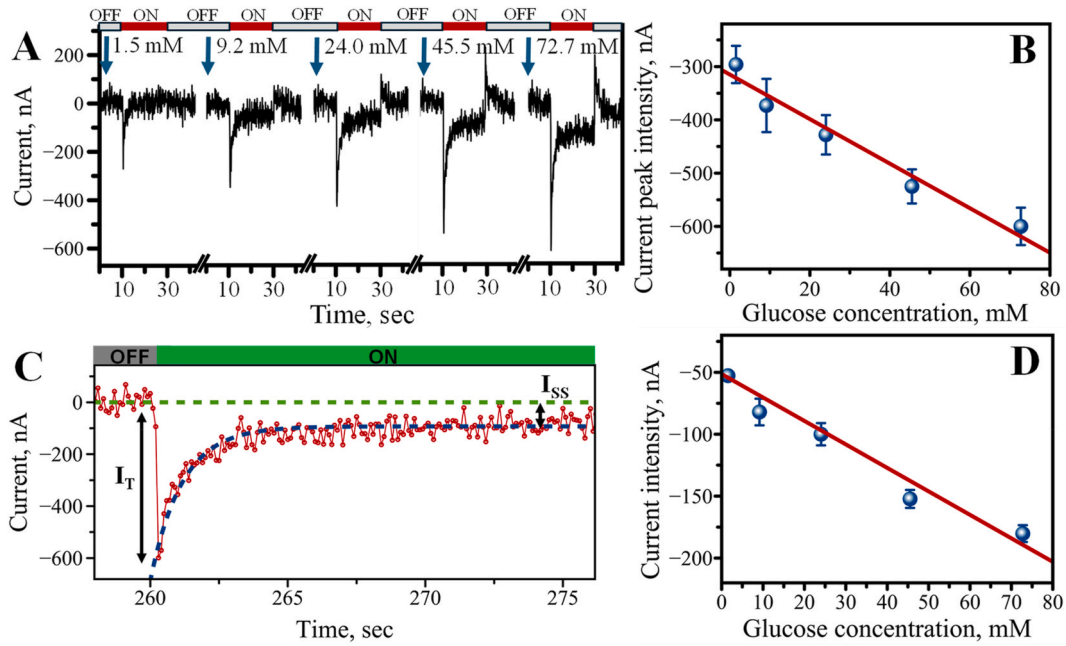

Fig. 3. (A) Time-dependent photocurrent response under oxygen-saturated conditions following glucose addition, with alternating 20-s light ON/OFF cycles. (B) A graph of the transient peak current I_T, as a function of glucose concentration, showing a linear relationship ($R^2 = 0.967$). C) Deconvolution of the light ON photocurrent into two components: a transient peak current (I_T), exhibiting exponential decay with an average time constant of 1.26 ± 0.12 s, and a steady-state current (I_{SS}) that stabilizes by the end of the 20-s illumination period. (D) A graph of the steady-state current (I_{ss}) as a function of glucose concentration, also fitted with a linear regression ($R^2 = 0.968$).

glucose concentrations, Fig. 3C. The first component is a transient peak current that emerges instantaneously when the light is turned on. This peak is characterized by a sharp initial spike, which rapidly decreases, following an exponential decay toward a stable current level, Fig. 3C. The decay dynamics was analyzed and quantified, yielding an exponential time constant ($\tau = 1.26 \pm 0.12$ s), averaged over multiple measurements, indicating consistent and reproducible behavior in all illumination cycles. The second component is the steady-state current, which is established towards the end of the 20-s light ON period. Similar to the transient peak, the steady-state current shows a clear dependence on glucose concentration. When plotted against glucose concentration, the steady-state current also produces a nearly linear dependence, as shown in Fig. 3D. Importantly, the steady-state current yields a limit of detection of 2.8 mM, nearly 4 times better sensitivity than that of the transient peak signal. The steady-state current thus offers a robust and reliable measure for glucose quantification. This LOD is slightly below the physiological fasting blood glucose range in adults (3.9–5.6 mM), allowing detection of normal fasting levels but remaining suboptimal for low-glucose measurements. As this is a proof-of-principle study, future optimizations of catalytic materials, electrode microarchitecture, and signal amplification are expected to significantly lower the LOD toward ideal clinically relevant performance. A possible improvement is the use of hydroquinone (HQ) as a redox mediator [17] which can boost photocurrent by providing a longer-lived, more stable electron shuttle than $^1O_2$; however, cyclic voltammetry and photocurrent measurements (Fig. S3, A and B) shows it is only effective at potentials below 0.2 V.

The transient behavior observed in the photocurrent is likely associated with the rapid generation and consumption of singlet oxygen upon illumination, followed by the system's return to a new equilibrium state. We propose that the two observed components of the signal correspond to non-faradaic and faradaic processes, both of which are exclusively triggered by light. This highlights the critical role of illumination in activating these processes and initiating the sensor's response. We attribute the initial sharp current peak to non-faradaic processes; specifically capacitive charging associated with the electrical double layer (EDL) quickly established across electrode/PCA/solution interface. Upon illumination, a rapid formation of singlet oxygen drives redistribution of charges resulting in a sudden photo-induced change in interfacial potential. This apparently results in the fast accumulation of charge in the EDL, storing energy transiently without net charge transfer across the interface. The sharp and instantaneous nature of this peak suggests a fast, light-induced redistribution of charges. Notably, a similar redistribution of charge also occurs when the light is turned off suggesting that singlet oxygen generation is essential for sustaining this capacitive behavior. In contrast, the second component, steady state current likely arises from faradaic processes, specifically charge transfer reactions occurring at the electrode interface. This current reflects ongoing electrochemical redox activity, such as the enzymatic oxidation of glucose catalyzed by GOx and the associated electron flow, as illustrated in Fig. 4B. Although further studies are required to unambiguously assign each current component to specific mechanistic pathways, the observed separation between capacitive (non-faradaic) and faradaic contributions provides valuable insight into the photodynamic behavior of the platform. This distinction may inform future design strategies aimed at optimizing both the sensitivity and energy efficiency of light-responsive biosensing platforms.

Fig. 4B illustrates the redox cycles responsible for electron flow in the presence of glucose. The flow proceeds in the opposite direction compared to glucose-free conditions shown in Fig. 2C. This shift accounts for the sensor's ability to generate a negative photocurrent upon glucose addition. When glucose is introduced, the enzyme-mediated oxidation of glucose by GOx is initiated. During this reaction, the flavin adenine dinucleotide (FAD) cofactor in GOx enzyme is reduced to $FADH_2$, altering the enzyme's redox state and enabling the conversion of glucose to glucono-δ-lactone. This process initiates a cascade of redox reactions involving GOx and singlet oxygen, as illustrated in Fig. 4B. Together, these coupled redox cycles collectively drive electron transfer toward the electrode, producing the observed negative photocurrent. Interestingly, although glucose oxidation itself is not light-dependent, the photocurrent appears only under illumination, emphasizing the critical role of the PSII-EY system and singlet oxygen in driving the electron flow.

To confirm that the primary driving factor of the negative photocurrent is singlet oxygen rather than dark-generated intermediates of the GOx + glucose reaction, a series of control experiments were performed. These tests rule out the possibility that the photocurrent arises from the photocatalytic oxidation of GOx-glucose reaction products upon illumination. The first control involved electrodes without GOx modification. When glucose was added – at concentrations that normally produce a negative photocurrent using GOx-modified electrodes – a positive current (~60 nA) was observed (Fig. S5A), similar to glucose-free response shown in Fig. 2A. Similar results were obtained when hydrogen peroxide was introduced, confirming that neither glucose nor the products of the GOx-glucose reaction induce the negative

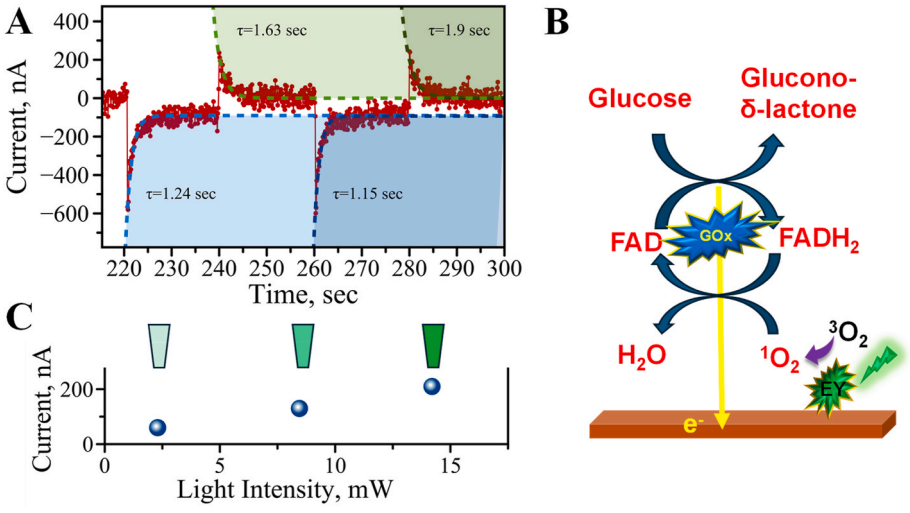

Fig. 4. (A) Time-dependent photocurrent traces fitted with exponential decay curves under laser ON (blue) and laser OFF (green) conditions. (B) Schematic illustration of the redox cycles responsible for electron transfer and the resulting negative current upon glucose addition. (C) Representative photocurrent response as a function of light intensity under oxygen-saturated conditions (see full dataset in Fig. S4A). (For interpretation of the references to colour in this figure legend, the reader is referred to the Web version of this article.)

photocurrent. Further evidence came from varying the dark ("off") intervals while keeping the illumination ("on") periods constant at 20 s for GOx-modified electrodes in glucose-containing solution. A negative photocurrent of -346 ± 22 nA was recorded for a 20 s dark interval, and the current magnitude remained essentially unchanged when other dark interval durations were tested (Fig. S5B). If the negative photocurrent originated from photooxidation of dark-generated products, longer dark intervals would have resulted in larger current amplitudes. The absence of such dependence strongly supports that singlet oxygen, rather than accumulated reaction products, drives the observed response. Although a detailed mechanistic picture remains to be fully elucidated, these results suggest that the system leverages $^1O_2$ to interact with GOx facilitating the regeneration of the enzyme's redox state, enabling a light-controlled, self-powered sensing process.

Another notable observation is the transient current response when the light is turned off. At the onset of each OFF cycle, a sharp peak in current appears instantaneously, followed by a rapid exponential decay toward zero, Fig. 4A. Analysis of this decay, performed similarly to the peak at the onset of ON cycle, yielded an average exponential time constant ($\tau = 1.68 \pm 0.42$ s) over multiple measurements. We hypothesize that this transient response reflects the discharge dynamics of the electrical double layer at the electrode interface as it returns to equilibrium, indicating a non-faradaic current. The sharp initial spike suggests a rapid release of accumulated charge, while the subsequent exponential decay is governed by interfacial charge redistribution.

A key feature of this platform is its ability to harness light energy and glucose oxidation as dual power sources, making it a strong candidate for self-powered diagnostic devices, especially in wearable and implantable formats. The sensor's dual contribution – steady-state enzymatic current and transient oxygen-related current – reveals the interplay between photochemical and biochemical processes, which enables sensing application. Additionally, the ability to fine-tune performance through light intensity enhances its adaptability and functionality. The sensor operates in two primary mechanisms of charge transfer: the direct reduction of singlet oxygen at the electrode and the enzymatic oxidation of glucose mediated by GOx. In oxygen-rich environments, the photocurrent exhibits a sharp rise followed by a decline to a stable level, indicative of the rapid kinetics of singlet oxygen generation and consumption. Under oxygen-depleted conditions, however, the steady-state current dominates. This observation suggests a rapid depletion of singlet oxygen near the electrode surface before stabilizing as the system reaches equilibrium.

The high reactivity of $^1O_2$ makes this approach particularly promising for developing photoactivatable sensors. By integrating light-sensitive components, the platform can utilize ambient or solar light for continuous self-powered operation. This might enable continuous physiological monitoring without frequent battery replacements reducing reliance on external power supplies. Such a combination offers significant potential for long-term health monitoring, real-time diagnostics, and next-generation wearable technologies.

3.4. Laser intensity dependence of the sensor's response

Amperometric measurements were performed to evaluate the sensor's response under varying 520 nm laser power settings (Fig. S4A). A noticeable increase in photocurrent was observed with higher laser power, especially when it exceeded 2.30 mW, suggesting a power threshold required for generating detectable photocurrent in the platform. As laser power increased, the photocurrent continued to increase steadily, reaching near-maximal levels as the power approached the maximum tested value of 14.20 mW, Fig. 4C. This trend demonstrates that sufficient light intensity is essential to activate the photosensitizer and effectively generate singlet oxygen ($^1O_2$). The results reveal a direct correlation between laser power and photocurrent, attributed to enhanced $^1O_2$ production at higher light intensities, which correlates with the increased availability of reactive species in the solution. This interplay between laser power and $^1O_2$ generation underscores the critical role of light intensity in modulating electron transfer dynamics within the system. These findings emphasize the importance of optimizing laser intensity as a controllable parameter to enhance the sensor's performance across different sample conditions.

3.5. Real samples analysis

To evaluate the real-world applicability of the developed sensing platform for glucose detection and its potential for self-powered operation, we tested the device performance using human sweat – a physiologically relevant and readily accessible biofluid that contains measurable levels of glucose [21]. Sweat serves as an ideal candidate for point-of-care and wearable diagnostics due to its non-invasive accessibility and its content of various key biomarkers, including glucose and lactate, which reflect metabolic activity, hydration status, and even stress [22]. In this context, sweat provided a natural source of glucose to activate the dual-mode functionality of the photosensitized biosensor, which integrates light-triggered singlet oxygen generation with enzymatic glucose oxidation. As shown in Fig. 5A, the addition of sweat in a volume equivalent to that used during calibration produced a well-defined photocurrent response (Fig. 5B). The sensor exhibited clear ON/OFF cycles corresponding to light exposure, closely resembling the sensor's behavior in pure glucose solutions, thereby confirming functional consistency even for complex biological samples. Notably, transient current peaks were observed in response to light modulation, characterized by a sharp negative spike upon light illumination (light ON) and a positive spike when the light was turned OFF. The maximum initial intensities of transient current peaks were -681 ± 60 nA (ON) and $+213 \pm 94$ nA (OFF), respectively. Both peaks are followed by characteristic exponential decay, stabilizing to a steady-state current within approximately 20 s. Fig. 5C presents a quantitative comparison of steady-state photocurrent intensities measured in sweat samples under argon-flushed (blue) and oxygen-saturated (red) conditions at the end of each illumination cycle, with error bars reflecting variability across multiple replicates. The recorded steady-state photocurrents were -106 ± 12 nA and -103 ± 10 nA, respectively, showing strong internal consistency and minimal variation across conditions. This close agreement suggests the sensor's robust performance in a biologically complex matrix and affirms its ability to generate reliable, interpretable signals. The reproducible photocurrent patterns observed across multiple measurements validate the sensor's operational stability and support its applicability for real-world biosensing in sweat. Furthermore, signal intensity remains largely unchanged over the sensor's operational timeframe (Fig. S4C), though improvements in long-term stability will be essential for developing a more robust sensing platform.

Overall, these results highlight the potential of the proposed system for integration into wearable devices aimed at continuous health monitoring. Indeed, the glucose-driven redox cycle offers a renewable and biocompatible energy source, but its long-term sustainability will depend on enzyme stability, substrate availability, and energy conversion efficiency. Future work will focus on optimizing sensor miniaturization and power management to fully leverage the self-powered capabilities enabled by glucose oxidation. Specifically, nanomaterial-based tuning of the electrode interfaces through catalytic enhancement and optimization of the surface area-to-volume ratio should promote a more efficient electron transfer and improve overall energy output. Additionally, strategies such as selective membrane coatings or microfluidic integration may be employed to enhance analyte specificity and sampling efficiency under dynamic, real-world conditions. By enabling multiplexed, autonomous operation in a compact form factor, this platform holds a significant promise for next-generation wearable biosensors.

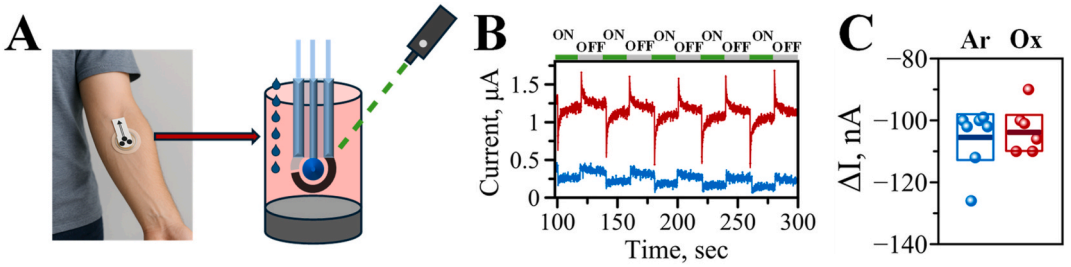

Fig. 5. (A) Collection of human sweat and its addition to the buffer-filled chamber containing the 3-electrode screen-printed electrode (3-SPE) setup; (B) Chronoamperometric responses following sweat addition under oxygen-saturated (red) and argon-flushed (blue) conditions, showing distinct light ON/OFF photocurrent behavior; (C) Comparison of corresponding steady-state photocurrent magnitudes for argon-flushed (blue), $\Delta I = -106 \pm 12$ nA, and oxygen-saturated (red), $\Delta I = -103 \pm 10$ nA, conditions, with error bars representing variability across multiple measurements. (For interpretation of the references to colour in this figure legend, the reader is referred to the Web version of this article.)

3.6. Sensor's operation depends on generation of singlet oxygen

Singlet oxygen generation is essential for the sensor's operation, as evidenced by its strict dependence on light exposure and the direct correlation between light intensity and photocurrent magnitude. The sensor functions in a chronoamperometric mode using disposable, screen-printed electrodes (SPEs), providing a scalable and cost-effective platform for detection. The photocurrent is triggered exclusively by light enabling precise on-off control that minimizes background noise and enhances analytical specificity, representing a shift toward controllable, light-activated biosensing systems. This light-triggered response links signal generation directly to the activity of Eosin Y (EY), a brominated fluorescein derivative embedded in the polymer layer near the electrode, Fig. 6B. EY is well-known for its efficient $^1O_2$ production, with broad use in applications such as photocatalytic water splitting and photo-redox catalysis [23]. By leveraging EY's photophysical properties, the biosensor introduces a novel, controllable approach to dynamic, light-gated detection. To confirm $^1O_2$ production by EY, we performed electron paramagnetic resonance (EPR) measurements using 1-hydroxy-3-carboxy-2,2,5,5-tetramethylpyrrolidine (CPH) as a spin-probe molecule. Upon irradiation with 520 nm light, which excites the $S_0 \rightarrow S_1$ transition in Eosin Y, a significant increase in the CPH radical signal was observed, indicating $^1O_2$ generation (Fig. 6A). After 2 min of irradiation, the EPR signal intensity rose sharply, displaying three characteristic peaks corresponding to the CPH radical, reaching intensity of 4.28×10^5 counts, while control samples (buffer and EY + CPH in buffer without irradiation) remained near baseline noise of 1.8×10^4 counts. Further confirmation came from the 9,10-anthracenediyl-bis(methylene) dimalonic acid (ABDA) assay, which selectively reacts with $^1O_2$ [24,25]. In an oxygen-saturated 50 μM EY solution, green light exposure caused ABDA absorbance at 400 nm to drop by 11.7 % in the first 40 s, from 0.351 to 0.310 (Fig. S6). Additional 40-s irradiation cycles led to further decreases, reaching 0.177, 0.096, 0.053, and finally 0.024 after the fifth cycle. Similar trends were observed at other characteristic ABDA absorption peaks (342, 359, and 378 nm), confirming sustained $^1O_2$ production. Together, the EPR and ABDA assays demonstrate Eosin Y's high efficiency as a Type II photosensitizer, a key property for the sensor's selective and light-activated signal generation. Upon excitation, EY undergoes intersystem crossing (ISC) to its triplet state, where it transfers energy to triplet oxygen ($^3O_2$) producing singlet oxygen ($^1O_2$), (Fig. 6C). This process is enhanced by the strong spin-orbit coupling of EY, as supported by TDDFT analysis (Supplementary Information). Molecular oxygen, in its ground state, exists as a triplet species O_2 ($^3\Sigma_g^-$) and can be excited to two singlet excited states, $^1\Delta_g$ ($^1O_2$) and $^1\Sigma_g^+$, with energies of 0.98 eV and 1.63 eV above the ground state, respectively [26]. This high energy of $^1O_2$ enables unique reactivity inaccessible to triplet oxygen, making it a crucial element of the sensor's light-gated functionality.

Leveraging the generation of singlet oxygen ($^1O_2$) by photosensitizers upon photoexcitation – is an innovative yet underexplored strategy in biosensing applications [15–17]. By enabling light-activated detection on demand, this approach offers significant potential for

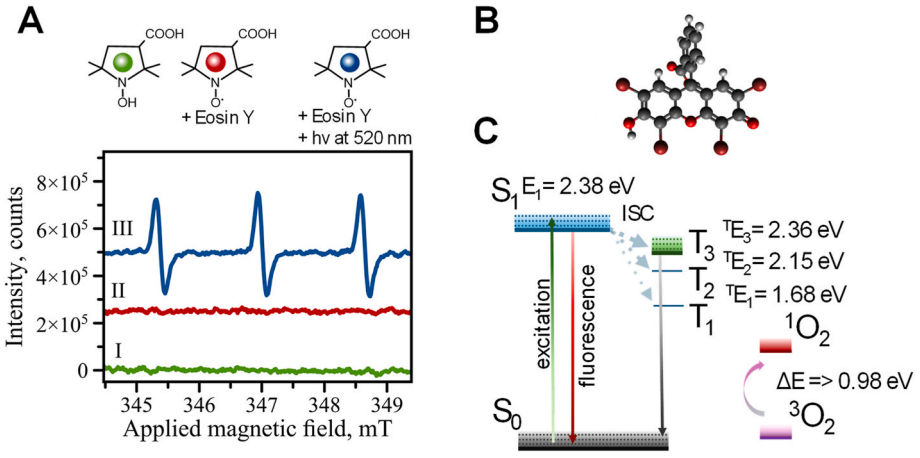

Fig. 6. A) EPR spectra of the CPH spin-trap molecule demonstrating generation of singlet oxygen by Eosin Y under various conditions: (I) buffer only, (II) CPH with Eosin Y, and (III) CPH with Eosin Y after 1 min irradiation at 520 nm light. Color coding corresponds to experimental conditions as shown in the top panel. B) Optimized molecular structure of Eosin Y. C) Schematic representation of the intersystem crossing, S_1- > T_n, a key step enabling singlet oxygen production (see detailed diagram in Supplementary Fig. S7). (For interpretation of the references to colour in this figure legend, the reader is referred to the Web version of this article.)

developing portable, energy-efficient diagnostic platforms. The sensor's functionality relies on the integration of photophysical and enzymatic components. Eosin Y, a type II photosensitizer embedded in a PCA polymer matrix, is photoexcited by light to transfer energy to molecular oxygen ($^3O_2$), converting it into reactive singlet oxygen ($^1O_2$). Critically, signal generation only occurs under light exposure, establishing $^1O_2$ production as a necessary trigger for detection. Optimization of $^1O_2$ production requires enhancing intersystem crossing (ISC) efficiency which promotes population of EY's triplet state, a prerequisite for energy transfer to $^3O_2$, Fig. 6C. The process depends on EY's strong spin-orbit coupling (SOC), which facilitates ISC from the first excited singlet state (S_1) to its triplet manifold. With a 0.98 eV energy threshold required to convert $^3O_2$ to $^1O_2$, the transition from the triplet (T) to the singlet ground state (S_0) must supply sufficient energy (Fig. 6B). Time-dependent density functional theory (TD-DFT) calculations (Fig. 6C) reveal three triplet states (T_1, T_2, and T_3) below the S_1, with E_{S1} = 2.38 eV (520 nm) and corresponding triplet energies of E_{T1} = 1.68 eV, E_{T2} = 2.15 eV, and E_{T3} = 2.26 eV. While all triplet states are energetically accessible via intersystem crossing, only the S_1 to T_3 transition exhibits sufficiently strong spin-orbit coupling for effective population of T_3. Spin-orbit coupling matrix elements (SOCME) show that S_1- > T_3 coupling is two orders of magnitude greater than that of S_1- > T_1 and S_1- > T_2 (as detailed in the Supplementary Information). Moreover, the small energy gap (ΔE = 0.02 eV) between E_{S1} and E_{T3} further promotes efficient ISC to the T_3 state, maximizing triplet population and, in turn, $^1O_2$ yield. To enhance sensor performance, design strategies should focus on increasing SOC strength and minimizing the singlet–triplet energy gap ($\Delta E_{S1\text{-}T3}$). These modifications can improve $^1O_2$ generation efficiency, advancing the development of light-responsive biosensors with high sensitivity and temporal control.

4. Conclusions

This study presents a light-activated biosensor that utilizes singlet oxygen generation for glucose detection, with strong potential for self-powered operation and integration into wearable diagnostic devices. By combining the Type II photosensitizer, Eosin Y (EY), with glucose oxidase (GOx), the sensor operates through a dual mode mechanism: photophysical activation under light exposure produces $^1O_2$, while enzymatic glucose oxidation drives redox reactions, generating a quantifiable electrochemical signal. The resulting photocurrent intensity shows a strong correlation with glucose concentration (R^2 = 0.97), with detection limits of 11.0 mM (transient peak current) and 2.8 mM (steady-state current). The platform utilizes a miniaturized three-electrode system, incorporating EY into a poly(pyrrole-2-carboxylic acid) (PCA) matrix to enhance photophysical activity and redox stability. Chronoamperometric measurements revealed distinct current responses depending on oxygen and glucose availability, with transient spikes in oxygen-rich conditions and a steady response in oxygen-depleted environments. Importantly, the present work represents a proof-of-principle demonstration of the light-driven sensing concept, intended to establish the fundamental mechanism and validate feasibility before full optimization for clinical performance. A key innovation of this platform is its light-triggered activation, which could eliminate the need for external power by harnessing light and glucose as dual energy inputs. Upon illumination, EY generates $^1O_2$ that initiates the sensing cascade, enabling autonomous, on-demand signal generation. By coupling light-driven redox chemistry with enzymatic catalysis, the sensor offers an energy-efficient solution for real-time, point-of-care diagnostics while significantly enhancing portability and usability. Crucially, the sensor demonstrated reliable performance in real biological samples. When tested with human sweat – a physiologically relevant, non-invasive biofluid – the device exhibited reproducible photocurrent responses consistent with those observed in glucose standards, validating its applicability for real-world conditions. This compatibility underscores the sensor's utility for continuous, noninvasive monitoring of metabolic biomarkers. Ongoing and future efforts will focus on miniaturization, expanding analyte specificity, and in vivo testing for real-time health monitoring and chronic disease management.

CRediT authorship contribution statement

Akhilesh Kumar Gupta: Writing – review & editing, Writing – original draft, Visualization, Validation, Methodology, Investigation, Formal analysis. **Robert Buller:** Writing – review & editing, Validation, Methodology, Investigation, Formal analysis. **Alexey V. Krasnoslobodtsev:** Writing – review & editing, Writing – original draft, Supervision, Resources, Project administration, Methodology, Funding acquisition, Formal analysis, Data curation, Conceptualization.

Declaration of competing interest

The authors declare the following financial interests/personal relationships which may be considered as potential competing interests: Alexey Krasnoslobodtsev reports financial support was provided by National Science Foundation. Alexey Krasnoslobodtsev reports financial support was provided by US Department of Energy. If there are other authors, they declare that they have no known competing financial interests or personal relationships that could have appeared to influence the work reported in this paper.

Acknowledgments

We acknowledge the following funding sources which partially supported this work (NSF DMR 2204027 and DOE-EPSCoR DE-SC0024284). Our team is grateful to the EPR core facility at the University of Nebraska Medical Center for their help with EPR measurements. TD-DFT calculations were performed utilizing the Holland Computing Center of the University of Nebraska, which receives support from the UNL Office of Research and Innovation, and the Nebraska Research Initiative.

Appendix A. Supplementary data

Supplementary data to this article can be found online at https://doi.org/10.1016/j.talanta.2025.129048.

Data availability

Data will be made available on request.

References

[1] A.K. Gupta, A.V. Krasnoslobodtsev, Fueling the future: the emergence of self-powered enzymatic biofuel cell biosensors, Biosensors 14 (2024) 316.
[2] C. Zhu, G. Yang, H. Li, D. Du, Y. Lin, Electrochemical sensors and biosensors based on nanomaterials and nanostructures, Anal. Chem. 87 (2015) 230–249.
[3] K. Promsuwan, A. Soleh, K. Samoson, K. Saisahas, S. Wangchuk, J. Saichanapan, et al., Novel biosensor platform for glucose monitoring via smartphone based on battery-less NFC potentiostat, Talanta 256 (2023) 124266.
[4] Y. Monsalve, A.F. Cruz-Pacheco, J. Orozco, Red and near-infrared light-activated photoelectrochemical nanobiosensors for biomedical target detection, Microchim. Acta 191 (2024) 535.
[5] M. Liu, J. Yang, J. Wang, Z. Liu, C. Hu, Light-addressable paper-based photoelectrochemical analytical device with tunable detection throughput for On-Site biosensing, Anal. Chem. 94 (2022) 583–587.
[6] A.H. Huynh Vo, V.C. Tran, T.T. Tran, T.T. Nguyen, A.D. Nguyen, M.H. Huynh Tran, et al., P-EcStat: a versatile design of photoelectrochemical and electrochemical sensing system with smartphone interface via bluetooth low energy, Appl. Sci. 14 (2024) 5420.
[7] A. Scott, S. Sakib, S. Saha, I. Zhitomirsky, L. Soleymani, A portable and smartphone-operated photoelectrochemical reader for point-of-care biosensing, Electrochim. Acta 419 (2022) 140347.
[8] G.-L. Wang, H.-J. Jiao, K.-L. Liu, X.-M. Wu, Y.-M. Dong, Z.-J. Li, et al., A novel strategy for the construction of photoelectrochemical sensors based on quantum

dots and electron acceptor: the case of dopamine detection, Electrochem. Commun. 41 (2014) 47–50.
[9] J. Shu, D. Tang, Recent advances in photoelectrochemical sensing: from engineered photoactive materials to sensing devices and detection modes, Anal. Chem. 92 (2020) 363–377.
[10] D. García-Fresnadillo, Singlet oxygen photosensitizing materials for point-of-use water disinfection with solar reactors, ChemPhotoChem 2 (2018) 512–534.
[11] Y. Wang, Y. Lin, S. He, S. Wu, C. Yang, Singlet oxygen: properties, generation, detection, and environmental applications, J. Hazard Mater. 461 (2024) 132538.
[12] A.A. Ghogare, A. Greer, Using singlet oxygen to synthesize natural products and drugs, Chem. Rev. 116 (2016) 9994–10034.
[13] B. Li, L. Lin, H. Lin, B.C. Wilson, Photosensitized singlet oxygen generation and detection: recent advances and future perspectives in cancer photodynamic therapy, J. Biophot. 9 (2016) 1314–1325.
[14] S.T. Shanmugam, R. Campos, S. Trashin, E. Daems, D. Carneiro, A. Fraga, et al., Singlet oxygen-based photoelectrochemical detection of miRNAs in prostate cancer patients' plasma: a novel diagnostic tool for liquid biopsy, Bioelectrochemistry 158 (2024) 108698.
[15] S. Trashin, V. Rahemi, K. Ramji, L. Neven, S.M. Gorun, K. De Wael, Singlet oxygen-based electrosensing by molecular photosensitizers, Nat. Commun. 8 (2017).
[16] P. Ling, X. Sun, N. Chen, S. Cheng, X. Gao, F. Gao, Electrochemical biosensor based on singlet oxygen generated by molecular photosensitizers, Anal. Chim. Acta 1183 (2021) 338970.
[17] S.T. Shanmugam, S. Trashin, K. De Wael, Singlet oxygen-based photoelectrochemical detection of DNA, Biosens. Bioelectron. 195 (2022) 113652.
[18] K.N. Ingenbosch, S. Quint, M. Dyllick-Brenzinger, D.S. Wunschik, J. Kiebist, P. Süss, et al., Singlet-oxygen generation by peroxidases and peroxygenases for chemoenzymatic synthesis, Chembiochem 22 (2021) 398–407.
[19] A.K. Gupta, A.V. Krasnoslobodtsev, DNA-templated silver nanoclusters as dual-mode sensitive probes for self-powered biosensor fueled by glucose, Nanomaterials 13 (2023).
[20] A. Kausaite-Minkstimiene, A. Kaminskas, A. Popov, A. Ramanavicius, A. Ramanaviciene, Development of a new biocathode for a single enzyme biofuel cell fuelled by glucose, Sci. Rep. 11 (2021) 18568.
[21] N. Promphet, C. Thanawattano, C. Buekban, T. Laochai, P. Lormaneenopparat, W. Sukmas, et al., Smartphone based wearable sweat glucose sensing device correlated with machine learning for real-time diabetes screening, Anal. Chim. Acta 1312 (2024) 342761.
[22] Y. Qiao, L. Qiao, Z. Chen, B. Liu, L. Gao, L. Zhang, Wearable sensor for continuous sweat biomarker monitoring, Chemosensors 10 (2022) 273.
[23] A. Lewandowska-Andrałojć, D. Larowska, E. Gacka, T. Pedzinski, B. Marciniak, How eosin Y/Graphene oxide-based materials can improve efficiency of light-driven hydrogen generation: mechanistic aspects, J. Phys. Chem. C 124 (2020) 2747–2755.
[24] T. Entradas, S. Waldron, M. Volk, The detection sensitivity of commonly used singlet oxygen probes in aqueous environments, J. Photochem. Photobiol. B Biol. 204 (2020) 111787.
[25] J.S. Nam, Y. Hong, C.G. Lee, T.I. Kim, C. Lee, D.-H. Roh, et al., Singlet oxygen generation from polyaminoglycerol by spin-flip-based electron transfer, JACS Au 2 (2022) 933–942.
[26] M. Bregnhøj, F. Thorning, P.R. Ogilby, Singlet oxygen photophysics: from liquid solvents to mammalian cells, Chem. Rev. 124 (2024) 9949–10051.